AD-A038 056   AIR FORCE WEAPONS LAB KIRTLAND AFB N MEX   F/G 20/8
                VACUUM PROPAGATION OF AN INTENSE RELATIVISTIC ELECTRON BEAM.(U)
                MAR 77   R B MILLER, D C STRAW
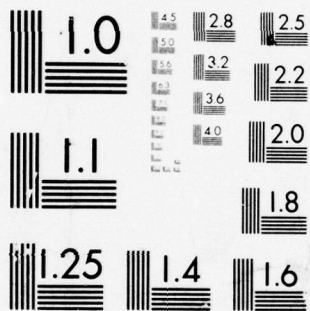
UNCLASSIFIED   AFWL-TR-76-156   NL
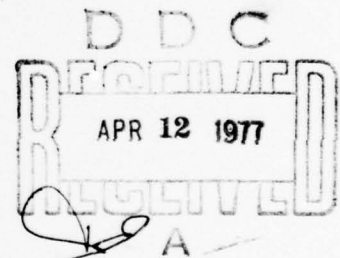
| OF |

AD
A038056

END

DATE
FILMED

4-77

1.0

4.5
5.0
5.6

2.8

2.5

1.1

3.2

2.2

3.6

4.0

2.0

1.8

1.25

1.4

1.6

MICROCOPY RESOLUTION TEST CHART
NATIONAL BUREAU OF STANDARDS-1963-A

ADA038056

VACUUM PROPAGATION OF AN INTENSE RELATIVISTIC ELECTRON BEAM

March 1977

Final Report

Approved for public release; distribution unlimited.

This final report was prepared by the Air Force Weapons Laboratory, Kirtland Air Force Base, New Mexico under Job Order 2301F101. Captain Robert B. Miller (DYS) was the Laboratory Project Officer-in-Charge.

When US Government drawings, specifications, or other data are used for any purpose other than a definitely related Government procurement operation, the Government thereby incurs no responsibility nor any obligation whatsoever, and the fact that the Government may have formulated, furnished, or in any way supplied the said drawings, specifications, or other data, is not to be regarded by implication or otherwise, as in any manner licensing the holder or any other person or corporation, or conveying any rights or permission to manufacture, use, or sell any patented invention that may in any way be related thereto.

This report has been reviewed by the Information Office (OI) and is releasabel to the National Technical Information Service (NTIS). At NTIS, it will be available to the general public, including foreign nations.

This technical report has been reviewed and is approved for publication.

ROBERT B. MILLER
Captain, USAF
Project Officer

THOMAS C. MAY
Major, USAF
Advanced Concepts Research Branch

FOR THE COMMANDER

JOHN S. DEWITT
Lt Colonel, USAF
Chief, Technology Division

REPORT DOCUMENTATION PAGE		READ INSTRUCTIONS BEFORE COMPLETING FORM
1. REPORT NUMBER AFWL-TR-76-156	2. GOVT ACCESSION NO.	3. RECIPIENT'S CATALOG NUMBER
4. TITLE *(and Subtitle)* VACUUM PROPAGATION OF AN INTENSE RELATIVISTIC ELECTRON BEAM.		5. TYPE OF REPORT & PERIOD COVERED Final Report.
		6. PERFORMING ORG. REPORT NUMBER
7. AUTHOR(s) Robert B. Miller, Capt, USAF David C. Straw		8. CONTRACT OR GRANT NUMBER(s)
9. PERFORMING ORGANIZATION NAME AND ADDRESS Air Force Weapons Laboratory (DYS) Kirtland Air Force Base, NM 87117		10. PROGRAM ELEMENT, PROJECT, TASK AREA & WORK UNIT NUMBERS 61102F 2301F101
11. CONTROLLING OFFICE NAME AND ADDRESS Air Force Weapons Laboratory (DYS) Kirtland Air Force Base, NM 87117		12. REPORT DATE March 1977
		13. NUMBER OF PAGES 44
14. MONITORING AGENCY NAME & ADDRESS*(if different from Controlling Office)*		15. SECURITY CLASS. *(of this report)* UNCLASSIFIED
		15a. DECLASSIFICATION/DOWNGRADING SCHEDULE

16. DISTRIBUTION STATEMENT *(of this Report)*

Approved for public release; distribution unlimited.

17. DISTRIBUTION STATEMENT *(of the abstract entered in Block 20, if different from Report)*

18. SUPPLEMENTARY NOTES

19. KEY WORDS *(Continue on reverse side if necessary and identify by block number)*

Intense relativistic electron beams
Collective ion acceleration
Virtual cathode

20. ABSTRACT *(Continue on reverse side if necessary and identify by block number)*

In this report the results of a series of electron beam vacuum propagation experiments are presented and compared with theoretical predictions. Important conclusions pertaining to time-dependent diode behavior, virtual cathode formation, and various equilibrium and stability criteria are reported.

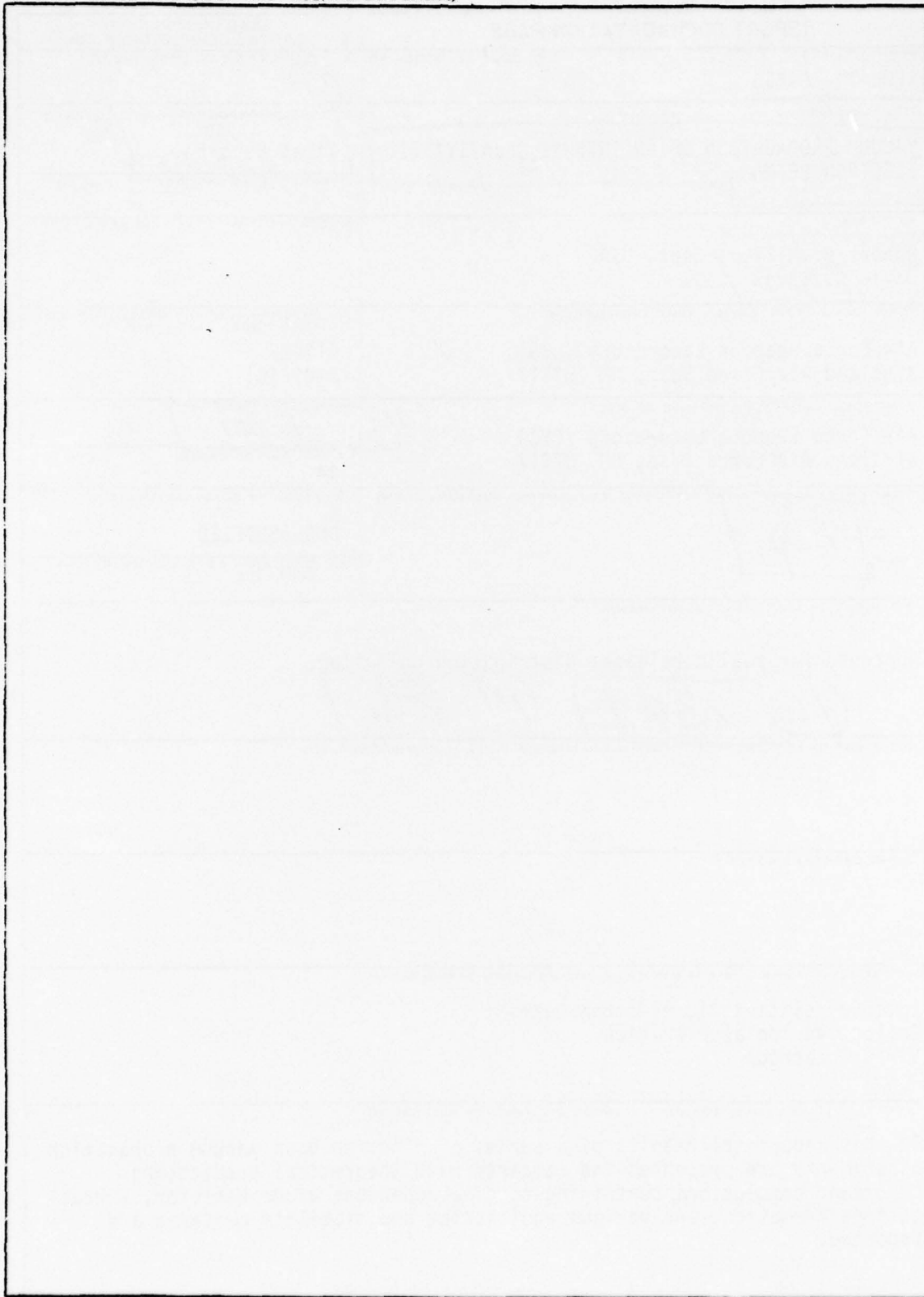DD $_{1\ JAN\ 73}^{FORM}$ 1473   EDITION OF 1 NOV 65 IS OBSOLETE

013150

CONTENTS

ILLUSTRATIONS

ILLUSTRATIONS (Continued)

SECTION I

INTRODUCTION

In several experiments with electron beams it is necessary to propagate an intense relativistic electron beam through an evacuated cylindrical guide tube along an externally imposed longitudinal magnetic field. Important examples include experiments involving microwave generation (references 1 through 5) collective ion acceleration (references 6 and 7), and autoacceleration (references 8 and 9). In other experiments initial propagation of an electron beam is not desired-- an important example again being collective ion acceleration (references 10 through 12).

Several previous studies of vacuum propagation have shown that for magnetic field strengths of the order of a few kilogauss the primary limitation to efficient transport of intense beams is the electrostatic potential depression which results from the electron beam space charge (references 13 through 19). If the injected beam current exceeds the space charge limiting current of the guide cavity a virtual cathode will form whose position and transparency are determined by several experimental parameters. It is also important to understand the conditions for stable equilibrium transport of beams which do not exceed the space charge limit. In this report we present several experimental observations pertaining to the injection of an intense electron beam into an evacuated drift space, including virtual cathode formation and space charge limited beam transport characteristics (beam spreading and beam loss) as a function of magnetic field strength for a variety of injection conditions. Brief discussions of selected portions of this work have been given elsewhere (references 20 and 21).

This report is organized as follows. Section II presents a brief summary of the theory pertaining to vacuum propagation, including virtual cathode formation and various equilibrium and stability criteria. Section III describes the experimental apparatus and the various diagnostics used to monitor the beam. Section IV contains the main experimental results. These are discussed with respect to the theory in section V, and pertinent conclusions are summrized in section VI.

SECTION II

THEORY

1. SPACE CHARGE LIMITING CURRENT

If it is assumed that the beam entering the cavity is mono-energetic and that all electrons move parallel to a very strong externally imposed longitudinal magnetic field, then the space charge potential problem (for the stationary case) reduces to the solution of Poisson's equation

$$\nabla^2 \phi = 4\pi e n \tag{1}$$

together with conservation of energy

$$(\gamma - 1)mc^2 - e\phi = (\gamma_0 - 1)mc^2 \tag{2}$$

and the equation of continuity

$$\nabla \cdot \underline{j} = 0 \tag{3}$$

In equations (1), (2), and (3) e and m are the charge and mass of an electron and c is the speed of light; n is the electron density, ϕ is the electrostatic potential, and $(\gamma - 1)mc^2$ is the electron kinetic energy (γ_0 corresponds to the injected energy). $\underline{j}$ is the current density defined by $\underline{j} = -en\underline{v}$, where $\underline{v}$ is the electron beam velocity vector.

Assuming cylindrical symmetry and combining equations (1) and (2) yields

$$\frac{1}{r} \frac{\partial}{\partial r} \left(r \frac{\partial \gamma}{\partial r} \right) + \frac{\partial^2 \gamma}{\partial z^2} = \frac{4\pi e^2 n}{mc^2} \tag{4}$$

With the assumed geometry, equation (3) reduces to

$$\frac{\partial}{\partial z} (n v_z) = 0 \tag{5}$$

6

or $j = -env_z = f(r)$ only. Recognizing that

$$\frac{v_z}{c} = \frac{(\gamma^2 - 1)^{1/2}}{\gamma} \tag{6}$$

and substituting into equation (4) yields

$$\frac{1}{r} \frac{\partial}{\partial r} \left(r \frac{\partial \gamma}{\partial r} \right) + \frac{\partial^2 \gamma}{\partial z^2} = - K \frac{\gamma}{(\gamma^2 - 1)^{1/2}} \tag{7}$$

where $K = \frac{4 \pi e j}{mc^3}$.

The solution of equation (7) subject to the appropriate boundary conditions describes the electron beam kinetic energy as a function of position in the cavity. It is important to note that the nonlinear right hand side of equation (7) has a singularity at $\gamma = 1$. Physically, if the electron beam current becomes too large, a virtual cathode forms which then divides the cavity into two regions. Equation (7) must then be solved in each region subject to the appropriate boundary conditions supplemented by the equation $\nabla \gamma = 0$ at the virtual cathode. For the general case the virtual cathode represents some inner boundary whose position and emission properties must be computed self-consistently.

There are several important special cases for which analytical solutions to equation (7) are known to exist. If the radius of the cavity becomes very much greater than the cavity length, then the geometry is essentially that of a gap between two infinite parallel planes perpendicular to the directed motion of the electron beam. This problem represents a generalization of the infinite planar diode case and has been examined by Voronin, et al. (reference 22). At the other extreme, when the length of the cavity is very much greater than the cavity radius, the geometry is that of a beam propagating in an infinitely long pipe which has been treated by Bogdankevich and Rukhadze (reference 23).

For the case of the beam in an infinitely long pipe, Olson has obtained a useful approximate expression for the space charge limiting current (corresponding to the onset of virtual cathode formation) by ignoring variations in the beam charge density due to the electrostatic potential (reference 24). For a uniform electron beam of radius r_b, current I_o, and kinetic energy $(\gamma_o-1)mc^2$ (i.e., no

radial variations in beam energy) propagating in a conducting tube of radius R, the approximate expression for the space charge limiting current is given by

$$I_{\ell o} = 8\left(\gamma_0 - 1\right)(mc^3/e)\left[1 + 2\,\ell n\left(R/r_b\right)\right]^{-1} \tag{8}$$

which compares with Bogdankevich and Rukhadze's interpolation result

$$I_{\ell o} = \left(\gamma_0^{2/3} - 1\right)^{3/2}(mc^3/e)\left[1 + 2\,\ell n\left(R/r_b\right)\right]^{-1} \tag{9}$$

A similar procedure is now used to obtain an expression for the space charge limiting current for a finite cavity. We wish to solve Poisson's equation, equation (1), subject to the boundary conditions

$$\phi(R,z) = \phi(r,o) = \phi(r,L) = 0 \tag{10}$$

where L and R are the length and radius of the cavity. The Green's function which satisfies the boundary conditions for such a cavity is given by (reference 25)

$$G(r,z;r',z') = \frac{8\pi}{R}\sum_{n=1}^{\infty}\frac{J_o\left(\lambda_n r/R\right)J_o\left(\lambda_n r'/R\right)}{\lambda_n\left[J_1\left(\lambda_n\right)\right]^2\sinh\frac{\lambda_n L}{R}}$$

$$\times\begin{cases}\sinh\left(\lambda_n z/R\right)\sinh\left[\lambda_n(L-z')/R\right], & z < z'\\[2mm]\sinh\left[\lambda_n(L-z)/R\right]\sinh\left(\lambda_n z'/R\right), & z > z'\end{cases} \tag{11}$$

Assuming a charge distribution given by

$$n(r',z') = \begin{cases}n_o, & 0 \leq r \leq r_b\\o, & r' \geq r_b\end{cases} \tag{12}$$

The potential as a function of position within the cavity is evaluated as

$$\phi(r,z) = 8\pi e n_o r_b R \sum_{n=1}^{\infty} \frac{J_o (\lambda_n r/R) J_1 (\lambda_n r_b/R)}{\lambda_n^3 \left[J_1(\lambda_n)\right]^2 \sinh (\lambda_n L/R)}$$

$$\times \left\{ \sinh \left[\lambda_n (L-z)/R\right] \cdot \left[\cosh (\lambda_n z/R) - 1\right] \right.$$

$$\left. + \sinh (\lambda_n z/R) \cdot \left[\cosh \left[\lambda_n (L-z)/R\right] - 1\right] \right\} \tag{13}$$

If a virtual cathode is not formed, the potential depression will be largest at the midpoint of the cavity (r=0, z=L/2). Evaluating $\phi(r,z)$ at this position yields

$$\phi_o (0, L/2) = 8\pi e n_o r_b R \sum_{n=1}^{\infty} \frac{J_1 (\lambda_n r_b/R)}{\lambda_n^3 \left[J_1 (\lambda_n)\right]^2} \left\{ 1 - \text{sech} \left(\frac{\lambda_n L}{2R}\right) \right\} \tag{14}$$

Setting the potential energy corresponding to ϕ_o equal to the e-beam kinetic energy yields the approximate expression for the limiting current of the cavity

$$I_{\ell o}^L = \frac{\beta (\gamma_o - 1) mc^3/e}{8} \left(\frac{r_o}{R}\right)$$

$$\times \left\{ \sum_{n=1}^{\infty} \frac{J_1 (\lambda_n r_b/R)}{\lambda_n^3 \left[J_1 (\lambda_n)\right]^2} \left[1 - \text{sech} \left(\frac{\lambda_n L}{2R}\right)\right] \right\}^{-1} \tag{15}$$

In the limit $L \to \infty$, $I_{\ell o}^L$ reduces to the usual expression

$$I_{\ell o}^{\infty} = \frac{\beta (\gamma_o - 1) mc^3/e}{1 + 2 \ln (R/r_b)} \tag{16}$$

In approximate terms, if the inequality

$$L/R \gtrsim 2.58 (r_b/R)^{0.133} \tag{17}$$

9

is not satisfied, the effect of the cavity end plates is important (>10%) and I^L_{2o} must be used to compute the limiting current of the cavity.

2. VIRTUAL CATHODE FORMATION

If the injected beam current exceeds the limiting current, the excess charge will be reflected back to the anode, or, if the magnetic field is not sufficiently strong, lost to the drift tube walls. The virtual cathode will emit a current in the forward direction whose equilibrium properties will be determined essentially by the strength of the longitudinal magnetic field for axial positions sufficiently removed from the virtual cathode region.

It is instructive to review the results of the one-dimensional (1-d) static theory for predicted trends for the position of the virtual cathode, and the magnitude of transmitted and reflected currents. Since the problem is an essentially time-dependent one, such a theory cannot lead to a correct solution; however, the static theory can provide a guide to regimes of behavior and it is used as such here.

For a drift gap of length L between two infinite parallel planes perpendicular to the direction of the motion of a homogeneous beam, the solution to equation (7) is

$$\sqrt{K (z - z_{min})^2} = f (\gamma, \gamma_{min}) \tag{18}$$

where the constant γ_{min} is the minimum value of the electron beam kinetic energy which occurs at the point $z = z_{min}$ in the drift space $0 \leq z \leq L$. The function $f(\gamma, \gamma_{min})$ is defined by

$$f(\gamma, \gamma_{min}) = \sqrt{2\gamma_{min}} \left\{ \frac{\sin\phi}{1+\cos\phi} \sqrt{1-k^2\sin^2\phi} \right.$$
$$\left. + (1-k^2) F (k,\phi) - E (k,\phi) \right\} \tag{19}$$

where $F(k,\phi)$ and $E(k,\phi)$ are the incomplete elliptic integrals of the first and second kind and

$$k^2 = \frac{1}{2} \left[1 - \sqrt{\gamma_{min}^2 - 1} \, / \, \gamma_{min} \right]$$

$$\phi = \text{arc cos} \; \frac{\gamma_{min} - \left[\sqrt{\gamma^2 - 1} - \sqrt{\gamma_{min}^2 - 1} \right]}{\gamma_{min} + \left[\sqrt{\gamma^2 - 1} - \sqrt{\gamma_{min}^2 - 1} \right]} \; ; \; 0 \leq \phi \leq \pi \tag{20}$$

Voronin's analysis of this problem indicates that a solution to equation (18) exists only for a limited range of K. In a certain interval $K_{\ell 1} \leq K \leq K_{\ell 2}$, there are two different solutions for each value of K; the possibility of virtual cathode formation ($\gamma_{min} = 1$) exists, but there is total transmission of the injected current. For $K > K_{\ell 2}$ there are no solutions and the stationary state with a virtual cathode and partial reflection of the current is the only possibility. For the planar geometry with equal potentials at the boundaries the transmitted current K_t and the position of the virtual cathode Z_{min} are determined from the injected current K, the gap spacing L, and the injected kinetic energy γ_0 according to

$$\left(2K - K_t \right)^{-1/2} + K_t^{-1/2} = 2 \, K_{\ell 1}^{-1/2}$$

$$Z_{min} = L \left\{ 1 - \frac{1}{2} \left(K_{\ell 1} / K_t \right)^{1/2} \right\} \tag{21}$$

where

$$K_{\ell 1} = \frac{4f^2 \, (\gamma_0, \, 1)}{L^2} \tag{22}$$

Defining the constants α, β, and δ according to

$$K = \alpha K_{\ell 1}$$

$$K_t = \beta K_{\ell 1}$$

$$Z_{min} = \delta L \tag{23}$$

11

equation (21) may be rewritten as

$$(2\alpha-\beta) = (2-\beta^{-1/2})^{-1}; \quad \delta = 1 = \frac{1}{2}\beta^{-1/2} \tag{24}$$

β and γ as functions of α are presented in figure 1. For the one-dimensional case as α is increased above 1, both the transmitted current (β) and the position of the virtual cathode (δ) change dramatically; as $\alpha \to \infty$, $\beta \to \frac{1}{4}$ and $\delta \to 0$. As the injected current is raised further and further above the limiting current ($K > K_{\ell 2}$), the transmitted current K_t decreases and the position of the vertical cathode Z_{min} approaches the anode. In addition, the _net_ current in the region between the anode and the virtual cathode is also described by K_t for the one-dimensional problem.
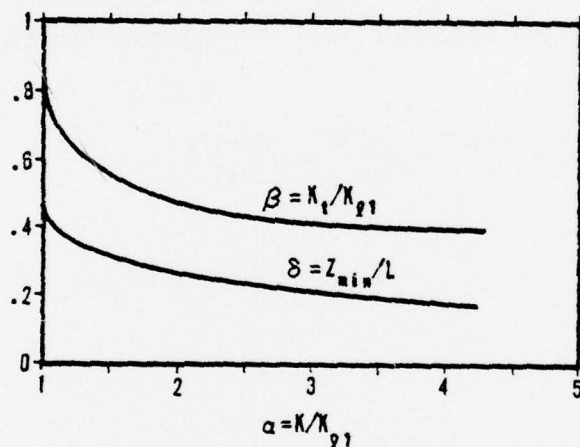
Figure 1. Transmitted Current (β) and the Position of the Virtual Cathode (δ) as a function of the Injected Current (α), From the 1-d Theory of Voronin, et al.

In going from one dimension to two and three dimensions, there will be quantitative differences (because the drift tube wall shorts the axial space charge field), but the qualitative results should remain the same. For example, there still exist two critical currents (corresponding to $K_{\ell 1}$ and $K_{\ell 2}$), but the difference between them decreases markedly on changing from one to two and three dimensions. Hence, in the stationary case with infinite longitudinal magnetic field the net current in the region between the virtual cathode and the anode should approximately equal the transmitted current. The value of the transmitted

12

current should be somewhat less than the limiting current, depending upon the value of the injected current.

Such results can be used to qualitatively explain certain observations relating to the structure of the space charge accelerating fields in collective ion acceleration experiments with intense electron beams. If the beam current only minimally exceeds the space charge limit $(I_0/I_{\ell o} \approx 1.1-1.3)$ the virtual cathode will form near the geometric center of the drift tube, and electrostatic fields of order $E_z \sim \dfrac{(\gamma_0-1)mc^2}{L/2}$, $E_r \sim \dfrac{(\gamma_0-1)mc^2}{R}$ will accelerate ions. In the usual experimental case $L > 2R$ and radially accelerated ions should predominate. On the other hand, if the injected current is much in excess of the space charge limit $(I_0 \gtrsim 2I_{\ell o})$, the virtual cathode will form much nearer the anode (approaching a distance from the anode of order c/ω_{pb} in the initial 1-d drift space limit (reference 26), and axially accelerated ions should predominate as experimentally observed (reference 11).

3. RIGID-ROTOR BEAM EQUILIBRIUM AND STABILITY

The condition for validity of the results of sections II.1 and II.2 is that electron motion be constrained to the axial direction only by the external application of a strong longitudinal magnetic field. One such criterion is that the energy associated with the external field greatly exceed the kinetic energy of the electron beam (reference 23), i.e.,

$$\frac{B_0^2}{8\pi} \gg n_e mc^2 \, (\gamma-1) \tag{25}$$

As this requirement is rather severe, it is also useful to present the sufficient condition for the existence of a rigid-rotor beam equilibrium and the stability thereof.

For an infinite, symmetric, relativistic electron beam propagating in vacuum parallel to a uniform external magnetic field, the radial force balance equation containing centrifugal, electrostatic, and magnetic forces is given by (reference 27)

$$\frac{m\gamma(r)v_\vartheta^2(r)}{r} = -e\left[E_r + \frac{1}{c}\left(v_\vartheta\,(B_0+B_z) - v_z\,B_\vartheta\right)\right] \tag{26}$$

13

In equation (26) E_r is the radial electric field as determined from Poisson's equation, B_0 is the externally applied magnetic field, and B_z and B_θ are the axial and azimuthal self-fields resulting from the azimuthal and axial beam velocity components, v_θ and v_z. In arriving at equation (26) it has been assumed that the ratio of the Larmor radius of the beam electrons r_L to the beam radius r_b is small (reference 28), i.e.

$$\frac{r_L}{r_b} = \frac{mc^2 \gamma \Delta\theta}{eB_z r_b} \ll 1 \tag{27}$$

where $\Delta\theta$ is the angular spread of beam electron velocities, e.g., from scatter in the anode foil.

If there is no axial velocity shear and if the azimuthal motion is non-relativistic so that the diamagnetic field contributions may be neglected, equation (26) reduces to

$$\gamma_0 \omega_\theta^2(r) + \frac{1}{r^2}(1 - \beta_0{}^2) \int_0^r dr' \; r' \; \omega_\rho{}^2(r') - \omega_\theta(r)\Omega = 0 \tag{28}$$

where

$$\omega_\theta = v_\theta/r$$

$$\gamma_0 = (1-\beta_z{}^2)^{-1/2} \approx (1-\beta_0{}^2)^{-1/2}$$

$$\Omega = (e\,B_0/mc)$$

and

$$\omega_\rho^2 = 4\pi n(r)e^2/m$$

where $n(r)$ is the beam density. Solving equation (28) for ω_θ yields

$$\omega_\theta^\pm(r) = \frac{\Omega}{2\gamma_0} \left\{ 1 \pm \left[1 - \frac{4}{\gamma_0 \Omega^2 r^2} \int_0^r dr' \; r' \; \omega_\rho{}^2(r') \right]^{1/2} \right\} \tag{29}$$

14

and the condition for the existence of an equilibrium is that the radical be real, or

$$\frac{4}{\gamma_0 \Omega^2 r^2} \int_0^r dr' \, r' \, \omega_\rho^2(r') \leq 1 \tag{30}$$

If this equilibrium condition is not satisfied, the beam will expand on the length scale ℓ according to

$$\ell = 2 \, \beta_0 \, c \, \gamma_0 \left\{ \frac{4}{\gamma_0 r^2} \int_0^r dr' \, r' \, \omega_\rho^2(r') - \Omega^2 \right\}^{-1/2} \tag{31}$$

For a beam with constant density out to a radius r_b, i.e.,

$$n(r) = \begin{cases} n_0 & ; \; 0 < r' < r_b \\ 0 & ; \; r_b < r' \end{cases} \tag{32}$$

equations (30) and (31) lead to the usual relationships (reference 13)
Equilibrium:

$$\gamma_0 \, \Omega^2 \geq 2 \, \omega_{\rho 0}^2 \tag{33}$$

Expansion length:

$$\ell = 2 \, \beta_0 \, c \, \gamma_0 \left\{ \frac{2 \omega_{\rho 0}^2}{\gamma_0} - \Omega^2 \right\}^{-1/2} \tag{34}$$

The equilibrium corresponding to equation (33) is the usual self-consistent rigid rotor equilibrium for which centrifugal forces are negligible, and the beam is only weakly diamagnetic, precessing nonrelativistically in the azimuthal direction. For beams which do not have constant electron density the equilibrium condition contains explicit radial dependence. At some values of radius the equilibrium condition may be satisfied, and at other values it may not be; in the latter case the beam will expand with scale length as given by equation (31) which also displays explicit radial dependence.

If the restrictions on the Larmor orbits of the beam electrons are relaxed, the resulting angular spread introduces two new effects: (1) a transverse kinetic pressure $P_L \sim nmc^2\gamma \, (\Delta\theta)^2$, and (2) variations in the electrostatic radial force. The existence of a beam equilibrium is not precluded, but the equilibrium differs in structure from that described by equation (33).

The rigid rotor beam equilibrium described above has been shown by Wong, et al. (reference 29) to be absolutely stable provided

$$\omega_{\rho o}^2 < 2 \; \gamma_o \; \Omega \; c/R \tag{35}$$

Equations (33) and (35) may be rewritten in terms of the magnetic field and beam current as

$$I < \left(\frac{\gamma_o e}{8mc}\right)(B \; r_b)^2 \tag{36}$$

$$I < \left(\frac{\gamma_o \; c \; r_b}{2R}\right)(B \; r_b) \tag{37}$$

These conditions in conjunction with the space charge current limit, equation (15), divide the beam current--magnetic field space into six regions in which different electron beam propagation characteristics are to be expected.

SECTION III

EXPERIMENTAL DESCRIPTION

The experimental configuration used in these studies is schematically presented in figure 2. The electron beam machine is an Ion Physics Corporation FX-25, a Van de Graaff charged 280-pF coaxial capacitor. For the experiments reported here, typical operating parameters are peak currents of 20 kA, peak electron beam kinetic energy of 2 MeV, with a pulse time of 40 nanoseconds. The voltage and current risetimes are of the order of 6 to 10 nanoseconds. Typical diode voltage and current traces obtained with a capacitive voltage divider and a resistive current shunt are shown in figure 3.

A diode extension assembly was constructed of thin-wall stainless steel so that the diode could be immersed in an approximately uniform axial magnetic field. The pressure in both the diode and the drift tube was maintained at $\sim 2 \times 10^{-5}$ Torr. The maximum background ion density that might be created at this pressure due to electron impact collisions is such that $(n_i \gamma^2 / n_e) \leqslant 10^{-2}$.

The diode geometry consisted of a 1.25 cm diameter flat tip aluminum cathode, a 0.0025 cm thick aluminum anode foil, and an anode cathode gap of 1.6 cm. For 2 MeV electrons passing through the anode foil the root-mean-square scattering angle is of the order of 4° to 6°.

The magnetic field was provided by the discharge of a 56 μF capacitor bank through a 330 μH solenoid. The period of the discharge was sufficiently long (0.85 μs) to allow complete field penetration through the drift tube (magnetic diffusion time on the order of 3 ns) and provided a constant magnetic field over the electron beam pulse duration. The different values of magnetic field (0 to 7.8 kG) were achieved by varying the relative timing between the capacitor bank and electron beam discharges using the delayed signal output of a Tektronix 555 oscilloscope. The maximum available longitudinal field strengths were at least twice as large as the highest intrinsic azimuthal beam magnetic fields.

Upon entering the drift tube, the beam was collimated with carbon apertures of various sizes to provide various beam radii and beam currents. Information about the radial profile of the entering beam was obtained by positioning a combination Faraday cup, carbon calorimeter immediately behind the carbon aperture and measuring the beam current and beam energy as a function of aperture diameter and magnetic field strength. Damage patterns on 0.0127 cm mylar films were also used to qualitatively monitor the entrance beam profile.
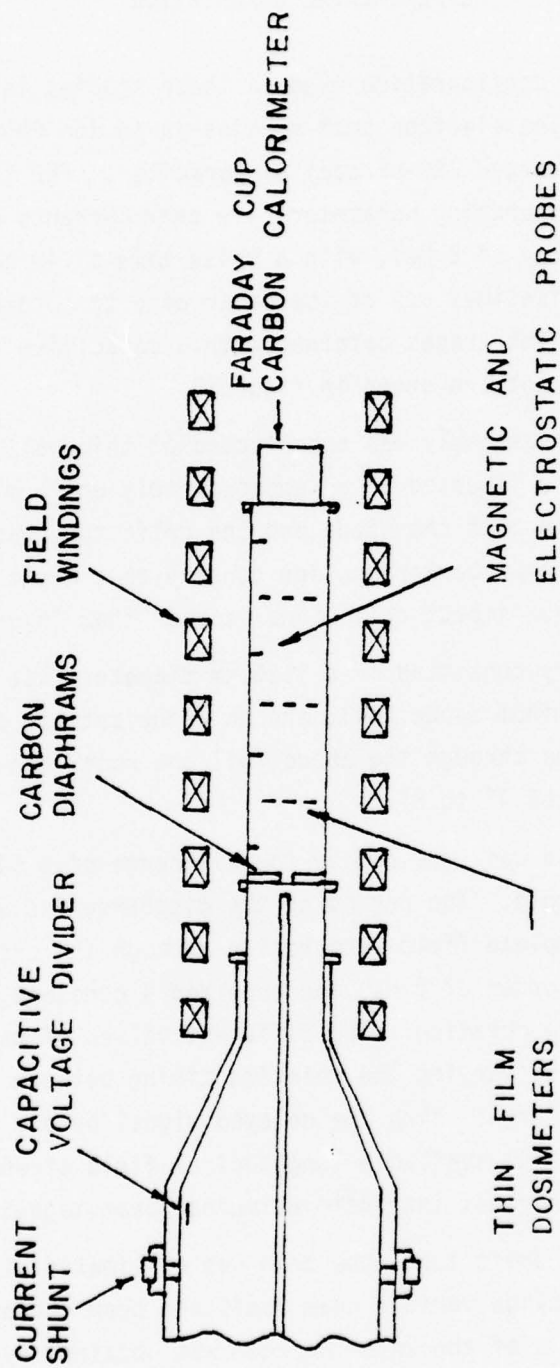
17

CURRENT
SHUNT

CAPACITIVE
VOLTAGE DIVIDER

CARBON
DIAPHRAMS

FIELD
WINDINGS

FARADAY CUP
CARBON CALORIMETER

MAGNETIC AND
ELECTROSTATIC PROBES

THIN FILM
DOSIMETERS

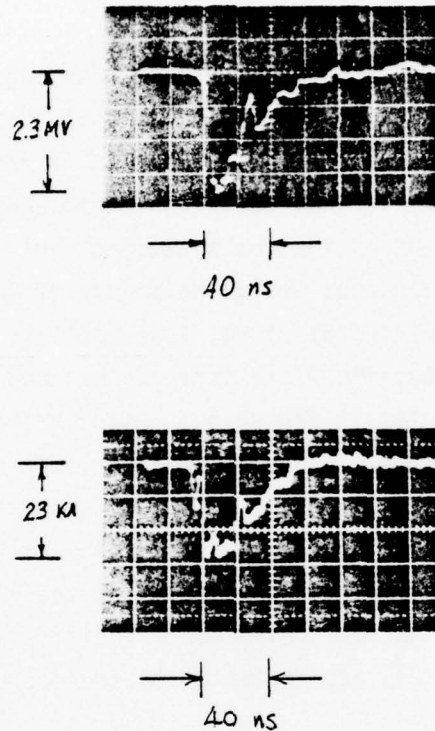Figure 2. Schematic of the Vacuum Propagation Experiment.

18

Figure 3. Typical FX-25 Diode Voltage and Current Waveforms.

The drift tube was constructed of 15.2 cm diameter thin-wall stainless steel tubing. The combination Faraday cup, carbon calorimeter located 50 cm from the anode monitored the transmitted beam current and beam energy. The length to radius ratio of the guide tube was sufficiently large that the endplate effects (equation (17)) were negligible. Further beam transport information was obtained from magnetic and electrostatic probes positioned at varying distances from the anode foil. Dye bleaching patterns on blue cellophane (reference 30) and rose cinemoid (reference 31) films were used to monitor the beam profile as a function of distance from the anode for varying magnetic field strengths. Variations in optical density due to electron beam induced bleaching were recorded by a scanning microdensitometer with a 6323 Å filter for the blue cellophane and a 5200 Å filter for the rose cinemoid.

SECTION IV

EXPERIMENTAL RESULTS

1. INJECTION CONDITIONS

As a result of aperturing the beam and varying the magnetic field strength a number of different injection conditions were possible; these are characterized by presenting the peak injected current as a function of magnetic field in figures 4(a), (b), and (c) for the various defining entrance apertures. The entrance current data, represented by the cross-hatched regions in the figures, indicate beam expansion in the diode; while the beam profile remained approximately constant across the defining aperture, less and less of the full machine current was injected as the magnetic field strength was decreased. (Representative current traces are presented in figure 5.) Also indicated on the graphs are the conditions corresponding to the space charge limit and beam equilibrium and stability from equations (15), (36), and (37). For our experimental parameters regions II and V were inaccessible upon injection of the beam into the drift space. Limitations on the range of validity of the rigid rotor equilibrium due to the angular spread of beam electron velocities arising from scatter in the anode foil (equation (27)) are indicated by the dashed lines in figure 4.

2. PEAK CURRENT TRANSMISSION

The results of transmission of the peak current in the pulse are indicated in figure 6, without regard to entrance aperture or changes in the beam radial profile during transport. The various regions of injection are indicated by the different symbols. Although a degree of scatter exists in the data, certain trends are apparent. For injected currents less than the space charge limit, the injected current is transported without loss except at very small values of the external magnetic field. On the other hand, when the injected current exceeds the space charge limit, the ratio of the transmitted current to the limiting current decreases as the ratio of the injected current to the limiting current increases. For comparison purposes, the results of the one-dimensional analytical theory of Vorovin, et al. are also presented.

3. BEAM ENERGY TRANSMISSION

The transmitted beam energy data are shown in figure 7, again without regard to entrance aperture or changes in the beam radial profile during transport. The normalization factor, W_ℓ, is the entrance beam energy for which the injected peak
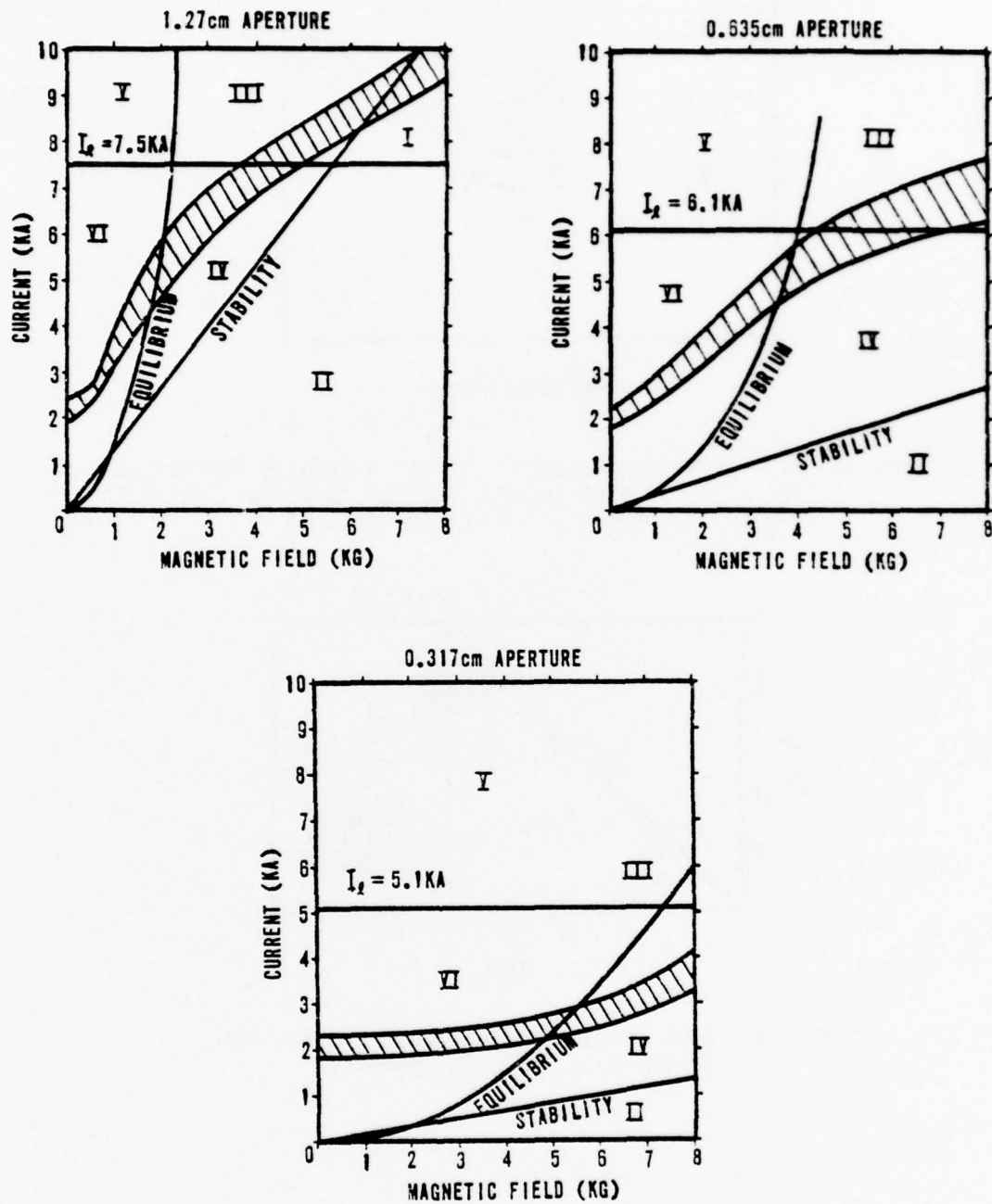
20

Figure 4. Peak Injected Electron Beam Current as a Function
of External Magnetic Field Strength: (a) 1.27 cm
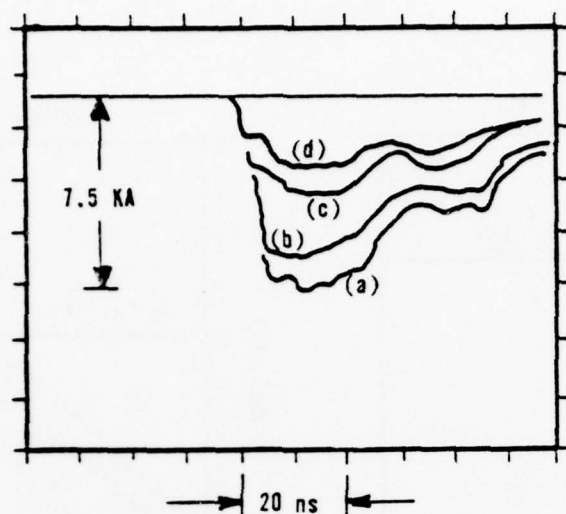Aperture; (b) 0.635 cm Aperture; (c) 0.317 cm.

Figure 5. Representative Injected Current Waveforms for Various
Magnetic Field Strengths, 1.27 cm Aperture: (a) 4.3
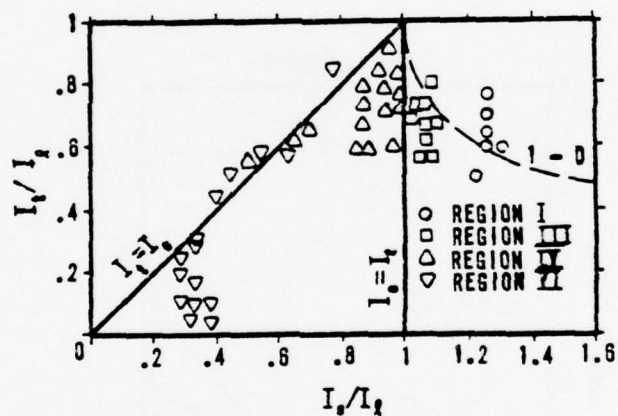kG; (b) 2.2 kG; (c) 1.1 kG; (d) 0.55 kG.

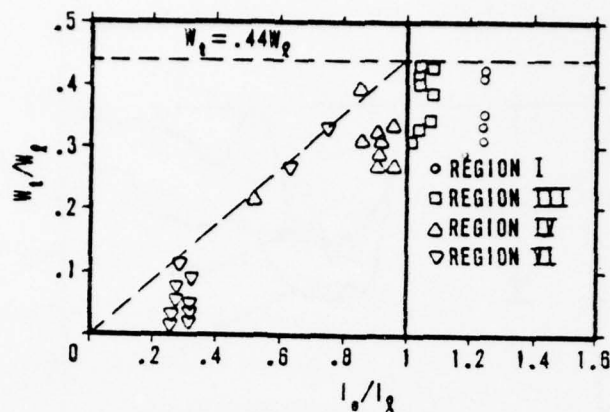Figure 6. Peak Transmitted Current as a Function
of the Peak Injected Current.

22

Figure 7. Transmitted Beam Energy as a Function
of the Peak Injected Current.

current was equal to the limiting current ($W_\ell(a)$ = 251J, $W_\ell(b)$ = 197J, and $W_\ell(c)$ = 161J.) As plotted, the transmitted beam energy data indicate the same qualitative features as the peak current transmission data; e.g., as the ratio of injected current to the limiting current is increased above unity, the transported beam energy decreases. However, in all cases the transported beam energy is substantially less than the injected beam energy. This result is substantiated by a comparison of the Faraday cup current waveforms taken at the entrance of the drift tube and at the end of the drift tube presented in figure 8. Evidently the transmitted energy corresponds to the energy associated with the peak current portion (FWHM $\approx$ 20 μs) of the injected current pulse; only a very small fraction of the late-time portion of the entrance current was transmitted.

4.   MAGNETIC PROBE RESULTS

Peak axial beam current measurements obtained with an integrated B_θ probe placed a distance of 3.18 cm from the anode foil are indicated in figure 9. For injected currents in excess of the space charge limit (regions I and III) the net current from the probe measurements is considerably less than the space charge limit and is approximately equal to the transmitted current as measured by the Faraday cup. For injection conditions such that the beam current is less than the space charge limit and the criterion for the existence of a beam equilibrium is not satisfied, the B_θ probe measurements are apparently erroneous because they indicate a net current far in excess of the injected current. Such a result could be caused by beam electrons moving radially across the weak longitudinal magnetic
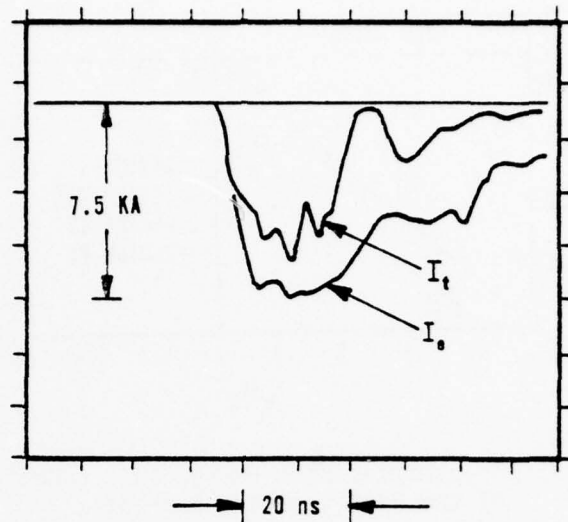
23

Figure 8. A Comparison of Injected and Transmitted Current
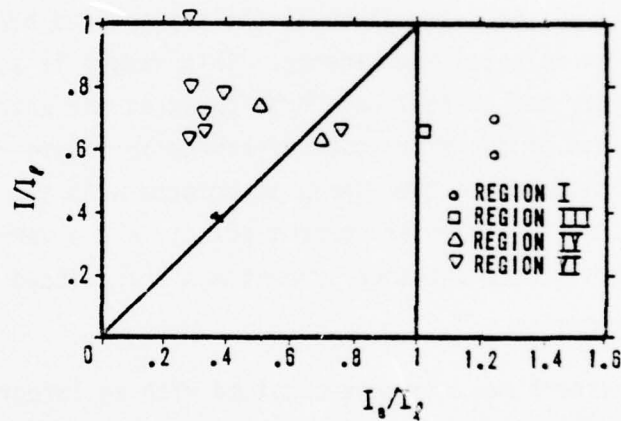Waveforms; 1.27 cm Aperture, B_θ = 4.3 kG.

Figure 9. B_θ Axial Beam Current Measurements as a
Function of Injected Beam Current.

field and striking the B_θ probe. Typical B_θ probe signals for the various re-
gions of injection criteria (figure 10) show marked differences on going from
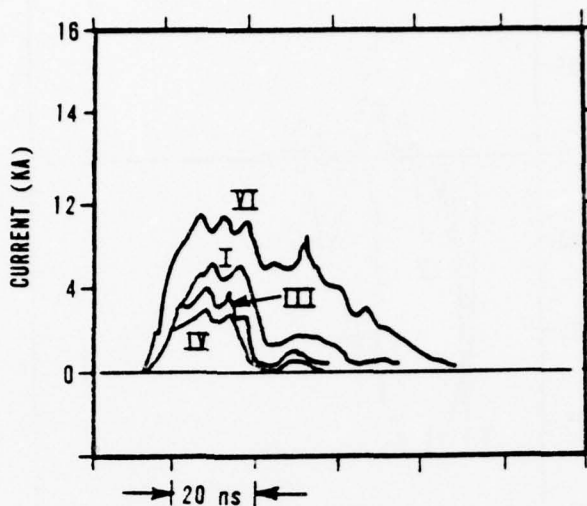regions I, III, and IV to region VI.

24

Figure 10. Typical B_θ Probe Waveforms for the Various Regions of Injection Criteria.

5. ELECTROSTATIC PROBE RESULTS

Electrostatic probe signals taken with probes of similar construction placed at various separations from the anode foil are presented in figures 11(a) through 11(d) for the different injection regions. Again, marked differences exist between the waveforms taken for injection regions I and IV and for injection region VI. The deviation from the usual electrostatic probe signal suggests that for injection region VI the electrostatic probes were acting as Faraday collectors for beam electrons moving radially across the field lines and striking the probes. The data for injection region I also suggest that the charge viewed by the electrostatic probe closest to the anode was substantially greater than the charge viewed by the other probes, suggesting reflection of beam electrons from a virtual cathode. Such a statement must remain qualitative, however, because the relative sensitivity of the various probes was not measured.

6. RADIAL BEAM PROFILE MEASUREMENTS WITH THIN FILM DOSIMETERS

Thin sheets of blue cellophane or rose cinemoid were placed directly in the path of the beam at varying distances from the anode foil for a variety of injection conditions. The bleaching of the thin films as measured by an optical densitometer can be related to the deposited electron beam dose and can provide information concerning the electron beam density (see the Appendix). Representative

25

Figure 11(a). Electrostatic Probe Waveforms for the Various Regions
of Injection Criteria. Probe Separation Distance
From the Anode Foil is 3.18 cm.

Figure 11(b). Electrostatic Probe Waveforms for the Various Regions
of Injection Criteria. Probe Separation Distance
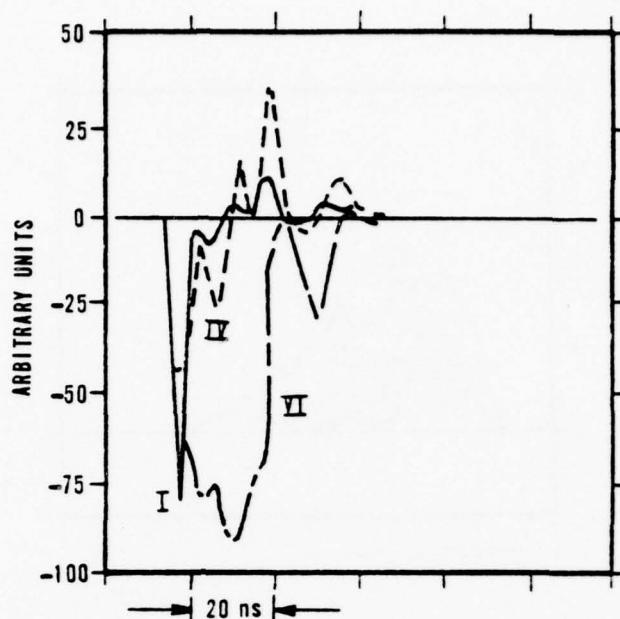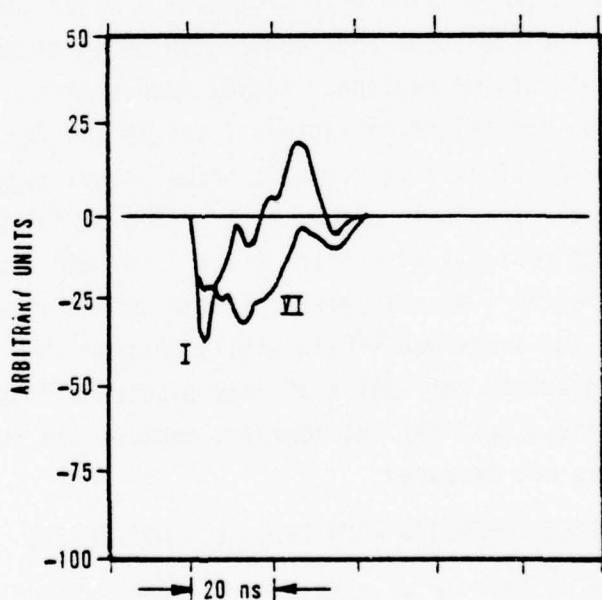From the Anode Foil is 18 cm.

26
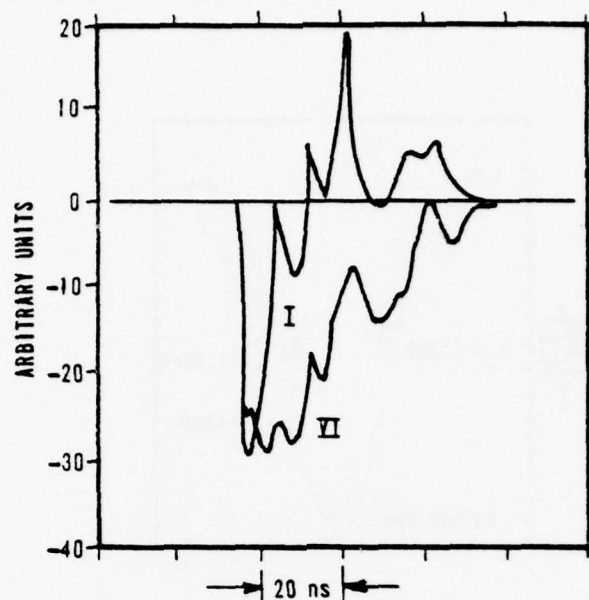
Figure 11(c). Electrostatic Probe Waveforms for the Various Regions
of Injection Criteria. Probe Separation Distance
From the Anode Foil is 33 cm.
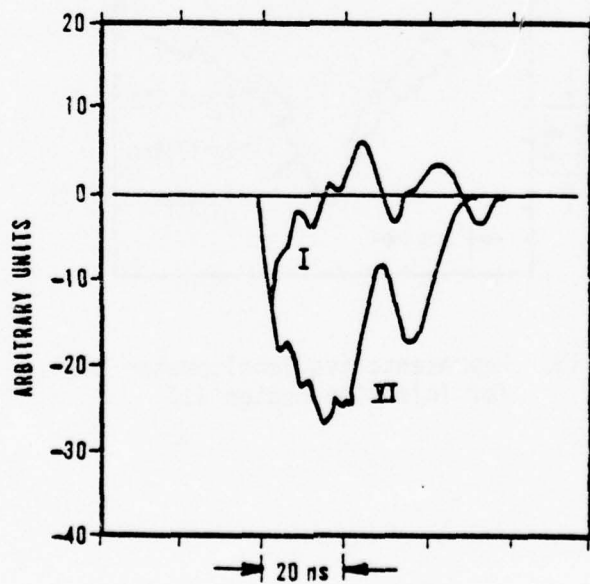
Figure 11(d). Electrostatic Probe Waveforms for the Various Regions
of Injection Criteria. Probe Separation Distance
From the Anode Foil is 48 cm.

27

densitometer scans for the various parameter regions of injection are presented in figures 12 through 16.

Figure 12.   Representative Densitometer Scans
for Injection Region I.

Figure 13.   Representative Densitometer Scans
for Injection Region III.
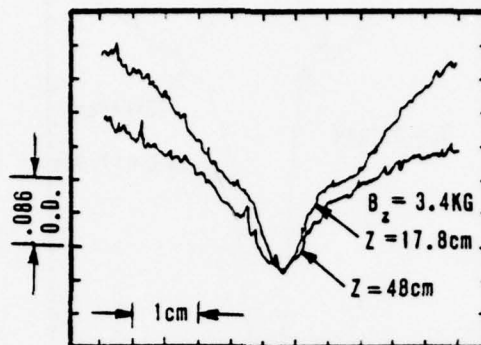
Figure 14.   Representative Densitometer Scans
for Injection Region IV.
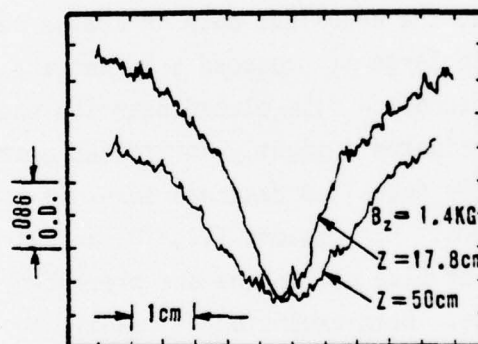
Figure 15.   Representative Densitometer Scans
for Injection Region VI.
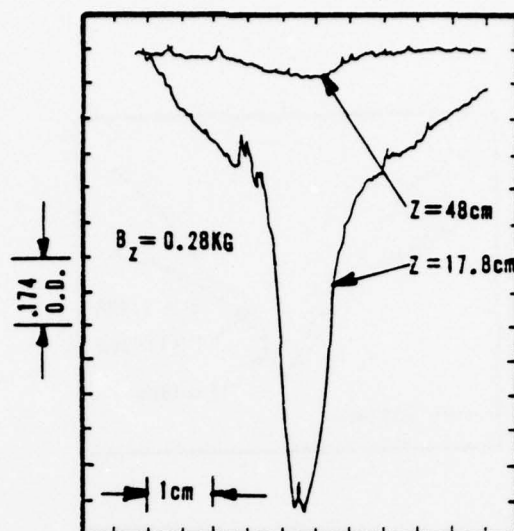
Figure 16. Representative Densitometer Scans for
Injection Far Into Region VI.

For region I (figure 12) the deposited dose in a blue cellophane film placed
3.18 cm from the anode was so large it produced a burned area corresponding
roughly to the entrance aperture. A film placed near the end of the drift tube
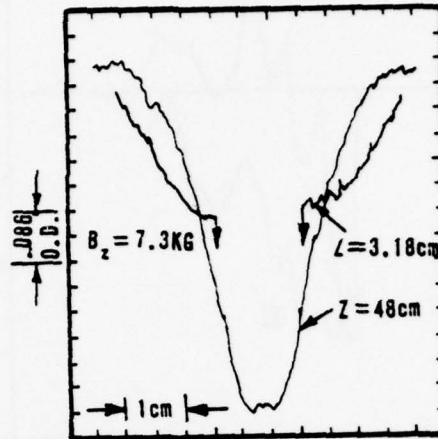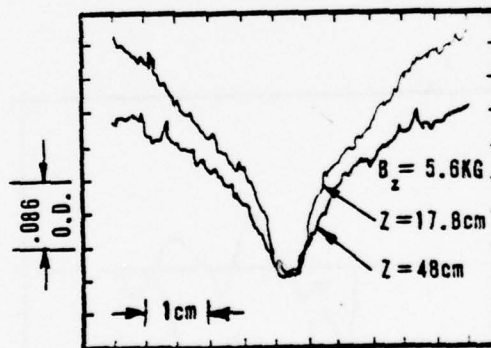48 cm from the anode also indicated a tightly collimated beam corresponding to
the entrance aperture, but the deposited dose was somewhat reduced and produced
only bleaching of the blue dye. For regions III, IV, and VI (figures 13 through
15), the densitometer scans of blue cellophane are presented such that the dose
maxima for the scans coincide. Beam expansion is readily apparent and becomes
more pronounced on going from region III to region VI. Far into region VI beam
expansion and loss of beam electrons to the drift tube wall necessitated the use
of the more sensitive rose cinemoid. Figure 16 (with densitometer baselines
aligned) indicates the severity of the expansion and beam loss.

SECTION V

DISCUSSION

Strong evidence for virtual cathode formation when the injected current exceeds the space charge limit exists in the data presented in figures 6 through 12. The maximum peak current and the total energy in the pulse are transmitted when the peak injected current is approximately equal to, or just less than, the space charge limit. As the ratio of injected current to the limiting current is increased above unity, both the transported peak current and the beam energy decrease approximately as predicted by the 1-d theory of Voronin, et al. Net current measurements by the B_θ probe and the bleaching of blue cellophane films placed near the anode indicate a substantial reflection of beam electrons from a virtual cathode, while electrostatic probe results indicate an apparent enhancement of the charge density in the same region.

Beam expansion was apparent when the stability criterion was not satisfied (compare figures 12 and 13), although the origin of such expansion is not entirely certain. As a result of electron reflection from the virtual cathode, the net azimuthal magnetic field will decrease and the radial electrostatic field will increase due to the increased space charge density necessitating a larger static axial magnetic field for radial force equilibrium. On the other hand, the expansion may arise from the development of an instability, the analysis of which has not been addressed.

On the basis of theoretical predictions (references 22 and 32) and recent computer simulations* some degree of beam hollowing was expected in this circumstance, but was not observed. Such results can most probably be attributed to the effects of transverse energy, and the fact that the maximum excess of the peak injected current above the space charge limit was minimal $(I_e/I_\ell \leqslant 1.25)$.

When the peak injected current was below the space charge limit beam expansion was always apparent, becoming more pronounced on going from injection region IV to region VI. (It should be noted that while injection region II was inacessible, for injection region I the current transmitted by the virtual cathode falls into region II.) Far into region VI loss of beam particles across magnetic field lines to the walls of the guide tube is evidenced in the probe data (figures 9, 10,

---

*Godfrey, B. B. and Poukey, J. W., Private Communications.

and 11), thin film dosimeter data (figure 16), and peak beam current and beam energy transmission data (figures 6 and 7). Zero-frequency cyclotron waves which should be produced when the beam is injected through an anode foil were not observed, although there were no specific attempts to do so. The existence of such waves, predicted in computer simulations of similar experiments,* could be harmful to various collective acceleration concepts, particularly autoresonant acceleration (reference 6) and could necessitate the use of foilless diodes (reference 33).

Since the electron beam generator used in these experiments produces only a pulsed beam and the equations presented in the previous sections are valid only for a steady-state current flow, it is necessary to examine the various time scales of interest in the problem. When the injected current exceeds the space charge limit the static solution concerning virtual cathode formation cannot be physical since it requires infinite charge density at the position of the virtual cathode. The physical solution is one in which the potential minimum and its location oscillate about their static values (reference 34). Previous calculations of the frequency of this oscillation indicated a value of the order of the beam plasma frequency depending on the magnitude of the reflected current (reference 35). Although recent 2-d numerical simulations have indicated a somewhat lower value,* the frequency is probably still so high for intense beams (of order 10^{10} to 10^{11} sec^{-1}) that such oscillations would be difficult to observe experimentally (perhaps only with rf power measurements using bandpass filters and solid state detectors). Oscilloscope traces should be expected to yield only the time averaged static solutions.

The time of flight of the beam through the 50 cm drift tube is ≤ 2 ns compared with the current risetime of order 10 ns. For our dimensions the energy expended in establishing the intrinsic magnetic field during the initial beam injection phase is not large enough to produce the beam self-destruction suggested by experiments using longer systems. Since the time of flight is much shorter than the relevant time scale for variations in the beam parameters it is expected that the steady-state formulas should be approximately valid at each instant of time.

---

*Godfrey, B. B., Private Communications.

32

Figure 17 presents a comparison of the corrected diode current pulse and the time dependent space charge limiting current computed from equation (9) using $\gamma(t)$ from the corrected diode voltage pulse. The diode current is normalized to the peak injected current data (figure 4(a)), in this case, the 1.27 cm diameter aperture at a field strength of 7.8 kG. As indicated, the injected current exceeds the space charge limit, implying the existence of a virtual cathode, over practically the entire pulse length. Based on the 1-d calculations of Voronin, et al., an estimate of the shape of the transmitted current pulse was made and is presented in figure 18, together with the actual transmitted current pulse for the same injection conditions. Considering the assumptions employed in the above arguments the agreement is remarkably good, quantitatively as well as qualitatively.
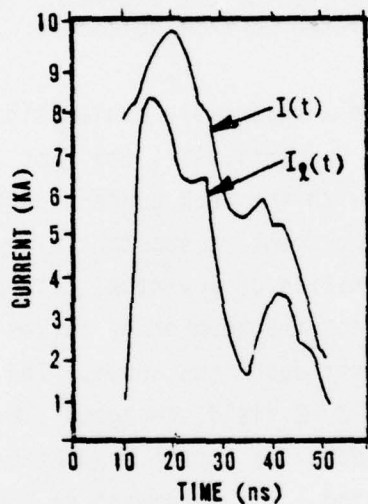

Figure 17. A Comparison of the Corrected Diode Current Pulse and the Time Dependent Space Charge Limiting Current for Injection Region I.
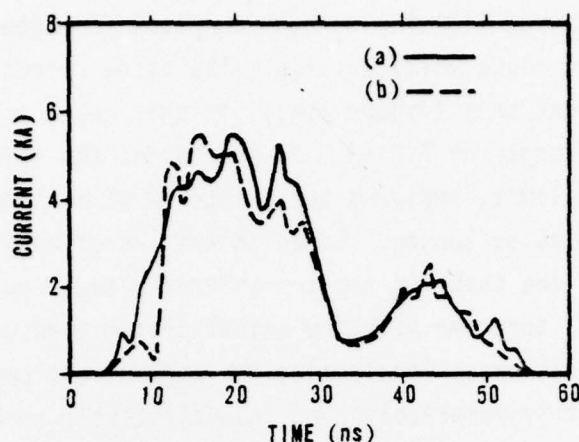
Figure 18. A Comparison of the Estimated (b) and Actual (a)
Transmitted Current Pulses for Injection Region I.

These results also provide a reasonable explanation for several of the ob-
servations presented earlier. In particular, the fact that the transported beam
energy corresponds so closely with the peak current portion of the injected cur-
rent pulse, even when the peak current is substantially below the space charge
limit, is due to late time formation of a virtual cathode. Figure 19 presents
the estimated transmitted current and beam power pulses based on the calculated
time dependent space charge limit described above. The injection conditions
(1.27 cm diameter aperture and 2 kG field strength) correspond to injection re-
gion IV . For comparison purposes the actual transmitted current as monitored by
the Faraday cup is also presented. The agreement is once again very good.

It is speculated that by properly designing the drift tube geometry it may
be possible to use the time-dependent generator-diode behavior (essentially diode
impedance) to create the condition for controlled motion of the virtual cathode
(reference 37). Such a development could have important implications for collec-
tive ion acceleration.

Major sources of error in these experiments arose from difficulties in accu-
rately specifying the injection conditions. From figures 4(a), (b), and (c) it is
evident that a decrease in the magnetic field strength increases the angular diver-
gence in the diode gap, and the expected range of validity of the stable rigid-
rotor equilibrium is uncertain. In addition, the current density is evidently not
constant across the beam. Since the magnetic field remained approximately con-
stant on going from the diode region to the drift tube region, it was not possible

34
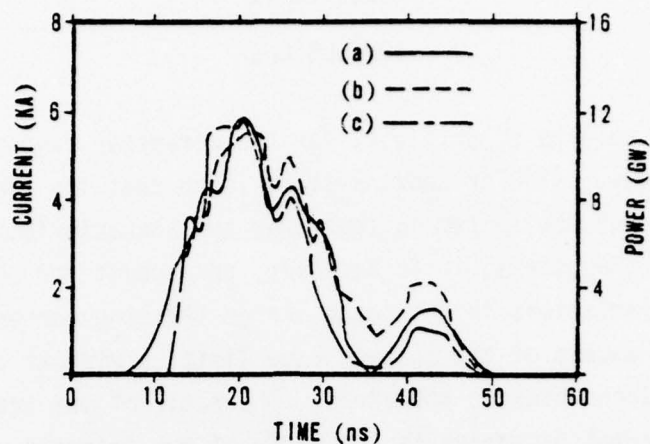
Figure 19. A Comparison of the Estimated Current (b) and
Power (c) Pulses, and the Actual Transmitted
Current Pulse (a) for Injection Region IV.

to isolate diode effects from drift tube effects, especially for the smaller
values of magnetic field strength. In future experiments such isolation might be
achieved through a nonadiabatic transition from a constant, uniform high field in
the diode to the desired field strength in the drift tube.

35

SECTION VI

CONCLUSIONS

The important results of this work for the parameter range explored can be summarized as follows. (1) For short systems (such that the time-of-flight of beam particles through the system is less than the characteristic time of variations in the beam parameters), it is necessary to account for changes in the beam parameters, e.g., variations in the space charge limiting current. (2) For injected currents in excess of the space charge limit, a virtual cathode forms and reflects beam electrons back to the anode. The ratio of the transmitted current to the limiting current decreases as the ratio of the injected current increases. (3) For injected currents less than the space charge limit, the injected current is transported without current loss and without beam expansion provided the magnetic field strength is in excess of the stability criterion. (4) As the field strength is reduced below the stability criterion, beam expansion occurs. The expansion becomes more pronounced as the field strength is decreased below the equilibrium criterion leading to severe loss of beam particles to the drift tube wall.

REFERENCES

1. Friedman, M. and Herndon, M., "Microwave Emission Produced by the Inter-
    action of an Intense Relativistic Electron Beam with a Spatially Modulated
    Magnetic Field," Phys. Rev. Lett., 28, 210-213, 1972.

2. Friedman, M., "Emission of Intense Microwave Radiation from an Auto-
    modulated Relativistic Electron Beam," Appl. Phys. Lett., 26, 366-367, 1975.

3. Pankratov, S. G., "Radiation of Electromagnetic Waves by a Modulated Elec-
    tron Beam," Sov. Phys. Tech. Phys., 19, 1248-1250, 1975.

4. Abramov, A. V., Panasynk, V. S., Pankratov, S. G., Samoshenkov, Yu. K.,
    Sokolov, A. A., and Stepanov, B. M., "Coherent Radiation from a Modulated
    Relativistic Electron Beam," Sov. Phys. Tech. Phys., 20, 121, 1975.

5. Granatstein, V. L., Sprangle, P., Herndon, M., Parker, R. K., and Schlesinger,
    S. P., "Microwave Amplication with an Intense Relativistic Electron Beam,"
    J. Appl. Phys., 46, 3800-3805, 1975.

6. Sloan, M. L. and Drummond, W. E., "The Autoresonant Accelerator Concept,"
    Phys. Rev. Lett., 31, 1234-1237, 1973.

7. Sprangle, P., Drobot, A. T., and Mannheimer, W. M., "Collective Ion Acceler-
    ation in a Converging Waveguide," Phys. Rev. Lett., 36, 1180-1183, 1976.

8. Friedman, M., "Autoacceleration of an Intense Relativistic Electron Beam,"
    Phys. Rev. Lett., 31, 1107-1110, 1973.

9. Siambis, J. G., "Autoacceleration of Intense Electron Beams by Coaxial
    Cavity Structures," NRL Memo Report, 1975.

10. Olson, C. L., "Theory of Ion Acceleration by Drifting Intense Relativistic
    Electron Beams, I. Theory; II, Comparison with Experiment," Phys. Fluids,
    18, 585-606, 1975.

11. Miller, R. B. and Straw, D. C., "Observations of Collective Ion Acceleration,"
    J. Appl. Phys.

12. Straw, D. C. and Miller, R. B., "Effects of High / Electron Beams for Collec-
    tive Ion Acceleration," J. Appl. Phys., To be published.

13. Andrews, M., Bzura, J., Fleischmann, H. H., and Rostoker, N., "Effects of a
    Magnetic Guide Field on the Propagation of Intense Relativistic Electron
    Beams," Phys. Fluids, 13, 1322-1327, 1970.

14. Mkheidze, G. P., Pulin, V. I., Raizer, M. D., and Tsopp, L. E., "Space-
    Charge Limited Current of an Uncompensated Relativistic Electron Beam,"
    Sov. Phys. JETP, 36, 54-55, 1973.

15. Friednam, M. and Hammer, D. A., "Catastrophic Disruption of the Flow of a
    Magnetically Confined Intense Relativistic Electron Beam," Appl. Phys. Lett.,
    21, 174-177, 1972.

16. Nation, J. A. and Read, M., "Limiting Currents in Unneutralized Relativistic Electron Beams," Appl. Phys. Lett., 23, 429-431, 1973.

17. Friedman, M., "Formation of a Virtual Cathode by a Relativistic Electron Beam Flowing Through a Cavity," Appl. Phys. Lett., 24, 303-305, 1974.

18. Abrachitov, Yu. I., Koidan, V. S., Konyukhov, V. V., Lagusov, V. M., Lukyanov, V. N., Mekler, K. I., and Ryutov, D. D., "Interaction of a High Intensity Relativistic Electron Beam with Plasma in a Magnetic Field," Sov. Phys. JETP, 39, 647-653, 1974.

19. Read, M. E. and Nation, J. A., "Space-Charge Limits in Unneutralized Relativistic Electron Beams," J. Plasma Phys., 13, 127-137, 1975.

20. Miller, R. B., Straw, D. C., and Kerns, J. R., "Propagation of an Uncompensated Relativistic Electron Beam in a Strong Magnetic Field," Bull. Am. Phys. Soc., 19, 965, 1974.

21. Miller, R. B. and Straw, D. C., "Vacuum Transport of an Intense Relativistic Electron Beam," Bull. Am. Phys. Soc., 20, 1324, 1975.

22. Voronin, V. S., Zozulya, Yu. T., and Lebedev, A. N., "Self-Consistent Stationary State of a Relativistic Electron Beam in a Drift Space," Sov. Phys. Tech. Phys., 17, 432-436, 1972.

23. Bogdankevich, L. S. and Rukhadze, A. A., "Stability of Relativistic Electron Beams in a Plasma and the Problem of Critical Currents," Sov. Phys. Vsp., 14, 163-179, 1971.

24. Olson, C. L. and Poukey, J. W., "Force-Neutral Beam and Limiting Currents," Phys. Rev., A9, 2631-2634, 1974.

25. Friedman, B., Principles and Techniques of Applied Mathematics, John Wiley and Sons, Inc., New York, 1966.

26. Poukey, J. W. and Rostoker, N., "One-Dimensional Model of Relativistic Electron Beam Propagation," Plasma Phys., 13, 897-904, 1971.

27. Davidson, R. D., Theory of Non-neutral Plasmas, W. A. Benjamin, Inc., Reading, Massachusetts, 1974.

28. Breizman, B. N. and Ryutov, D. D., "Powerful Relativistic Electron Beams in a Plasma and in a Vacuum (Theory)," Nuc. Fusion, 14, 873-907, 1974.

29. Wong, H. V., Sloan, M. L., Thompson, J. R., and Drobat, A. T., "Stability of an Un-neutralized Rigidly Rotating Electron Beam," Phys. Fluids, 16, 902-903, 1973.

30. Henly, E. J. and Richman, D., "Cellophane-Dye Dosimeter for 10^5 to 10^7 Roentgen Range," Anal. Chem., 28, 1580-1582, 1956.

31. Menkes, C. K. and Goldstein, N., "Color Films for Megarad Dosimetry," USNRDL-TR-1097, 1966.

32. Agafonov, A. V., Voronin, V. S., Lebedev, A. N., and Pazin, K. N., "Magnetic-Field Transport of a High-Current Electron Beam," Sov. Phys. Tech. Phys., 19, 1188-1192, 1975.

33. Friedman, M. and Ury, M., "Production and Focusing of a High Power Relativistic Annular Electron Beam," Rev. Sci. Instrum., 41, 1334-1335, 1970.

34. Dunn, D. A. and Ho, I. T., "Computer Experiments on Ion-Beam Neutralization with Initially Cold Electrons," AIAA Journal, 1, 2770-2777, 1963.

35. de Jagher, P. C., Hopman, H. J., and Jurgens, B., "The Formation of Virtual Cathodes with Relativistic Electron Beams," Proc. 12th Int'l. Conf. Phenomena in Ionized Gases, 342, 1975.

36. Friedman, M. and Siambis, J. G., "Conditions for the Self-Destruction of a Pulsed Intense Relativistic Electron Beam," Appl. Phys. Lett., 28, 308-311, 1976.

37. Miller, R. B., "Collective Ion Acceleration by the Controlled Motion of the Virtual Cathode," AFWL Tech. Rept., AFWL-DYS-TN-75-113, 1975.

38. Evans, R. D., The Atomic Nucleus, McGraw-Hill, 1955.

APPENDIX

ANALYSIS OF ELECTRON BEAM DOSE PROFILES IN
ROSE CINEMOID AND BLUE CELLOPHANE

INTRODUCTION

The radial profile of the electron beam was measured for a variety of injection conditions by placing thin sheets of cinemoid or blue cellophane directly in the path of the beam at varying distances from the anode foil. The bleaching of the thin films as measured by an optical densitometer can be related to the deposited electron beam dose, and with certain assumptions this information can be used to infer the electron beam density profile.

The electron dose may be defined as the number of electrons passing through a given volume multiplied by the energy loss per electron. Assuming cylindrical symmetry, the number of electrons passing through the thin film of thickness ΔZ in the area $r \Delta r \Delta \theta$ is given by $n(r) r \Delta r \Delta \theta v \Delta t$ where v is the electron velocity and Δt is the pulse time. If ΔE is the energy loss per electron, then the beam density is related to the deposited dose $D(r)$ in the volume element $r \Delta r \Delta \theta$ according to

$$n(r) = \frac{\Delta Z}{v \Delta t} \frac{D(r)}{\Delta E} \tag{A1}$$

From Evans (reference 38) the stopping power for electrons in the thin films is related to the stopping power in air according to

$$\frac{dE}{dx}\bigg|_f \approx \frac{\rho_f}{\rho_{air}} \left(\frac{dE}{dx}\right)_{air} \tag{A2}$$

Over the electron energy range of 0 to 10 MeV, a good approximation for $\frac{dE}{dx}\big|_{air}$ is

$$\frac{dE}{dx}\bigg|_{air} \simeq \frac{1.46}{\beta^2} \frac{keV}{cm} \tag{A3}$$

where $\beta = v/c$. For relativistic electrons $v \approx c$, and the energy lost by an electron in the foil thickness ΔZ is given by

$$\Delta E \approx 1.46 \ (\Delta Z) \ (\rho_f/\rho_{air}) \ (keV) \tag{A4}$$

where $\rho_{air} = 1.29 \times 10^{-3}$ g/cm^3.

The unit of dose is the rad defined by

$$1 \ rad = 100 \ erg/gm \tag{A5}$$

Taking into account the density of the film material, a convenient formula is

$$1 \ rad = 6.25 \times 10^7 \ \rho_f \ MeV/cm^3 \tag{A6}$$

After irradiation the films were scanned with an optical densitometer. The definition of optical density is

$$OD = \log_{10} \frac{I_o}{I_x} \tag{A7}$$

where I_o is the intensity of the light source and I_x is the light intensity after passage through the thin film. Two other definitions are also useful when using calibration curves to determine observed dose. If I_1 is the light intensity passing through an unirradiated film and I_2 is the light intensity passing through an irradiated film, the negative charge in optical density is defined by

$$(-\Delta OD) = \log_{10} \frac{I_2}{I_1} \tag{A8}$$

and the change in percent transmission is defined as

$$\Delta = (I_2 - I_1)/I_o = 10^{-OD_1} \left(10^{(-\Delta OD)} - 1 \right) \tag{A9}$$

42

BLUE CELLOPHANE CALIBRATION

The thin (.001 in.) blue cellophane film used in these experiments is a sandwich structure with a core of regenerated cellulose doped with the sodium salt of dimethoxy diphenyl diago bis. The radiation chemistry which occurs when the film is irradiated is still not well understood. The hypothesis is that the radiation produces radicals via ionizing interactions with the cellophane. These radicals, along with intermediate radical states, then chemically react with the dye producing the bleaching effect.

A typical calibration curve for blue cellophane obtained with an intense pulsed electron beam machine is shown in figure A1. The dose rate was in the range of 10^{15} rads/sec. By simultaneously exposing the blue cellophane and reading a standard diagnostic (in this case an aluminum calorimeter) the cellophane was directly calibrated in terms of electron dose. To use the calibration curve it is necessary to convert rads (equation (A1)) to rads (blue cellophane) and to convert change in transmission to change in optical density (equation (A9)).
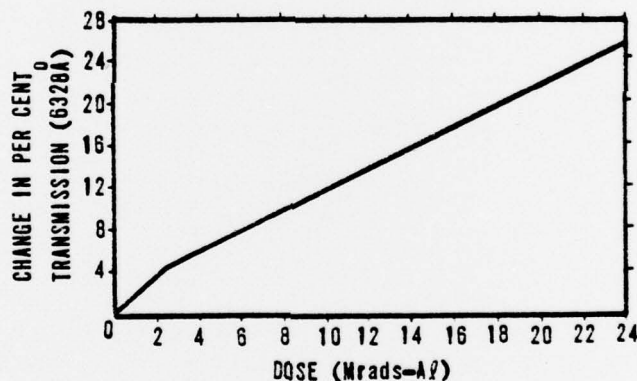

Figure A1.   Dose Calibration Curve for the Blue
Cellophane Thin Film Dosimeter.

ROSE CINEMOID CALIBRATION

Cinemoid is the trade name of a series of dyed plastics used in theatrical lighting. One of the series, No. 48 bright rose, has been found to be a useful medium for measuring X-ray, γ-ray, and electron exposures. The calibration curve for rose cinemoid for pulsed electron beams is presented in figure A2.
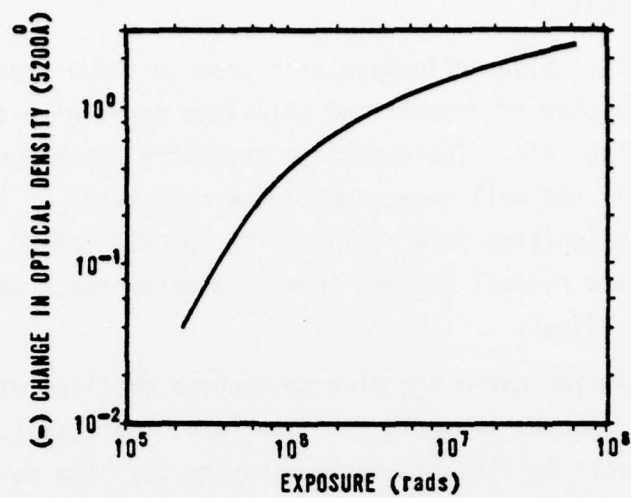
Figure A2. Dose Calibration Curve for the Rose
Cinemoid Thin Film Dosimeter.